Polarized thermal dust emission as seen by Planck : A comparison with MHD simulations and lessons from a toy model

Planck Collaboration, F. Levrier, J. Neveu

LERMA, Observatoire de Paris, PSL Research University, CNRS, Sorbonne Universités, UPMC Univ. Paris 06, École Normale Supérieure, F-75005, Paris, France

Abstract

The **Planck** satellite has mapped the polarized microwave sky (from 30 GHz to 353 GHz) with unprecedented sensitivity and angular resolution. This wealth of data yields **the first complete map of polarized thermal emission from dust in our own Galaxy**, shedding new light on the formation of dense cold structures within which new stars and planetary systems are born, under the combined effects of gravity, turbulence and magnetic fields. We present **a statistical analysis of this polarized emission from nearby molecular clouds**, with an emphasis on the evolution of the maximum polarization fraction observed as a function of column density, and on the anti-correlation between the polarization fraction and the local dispersion of polarization angles. To interpret this data, **numerical simulations of anisotropic MHD turbulence underline the essential role played by the topology of the interstellar magnetic field**, in particular its large-scale component. As an extension to this work published in **Planck Intermediate Results XX** (A&A, 576, 105, 2015), **the statistical properties of the random component of the interstellar magnetic field are explored** using a toy model based on fractional Brownian motion (fBm) fields.

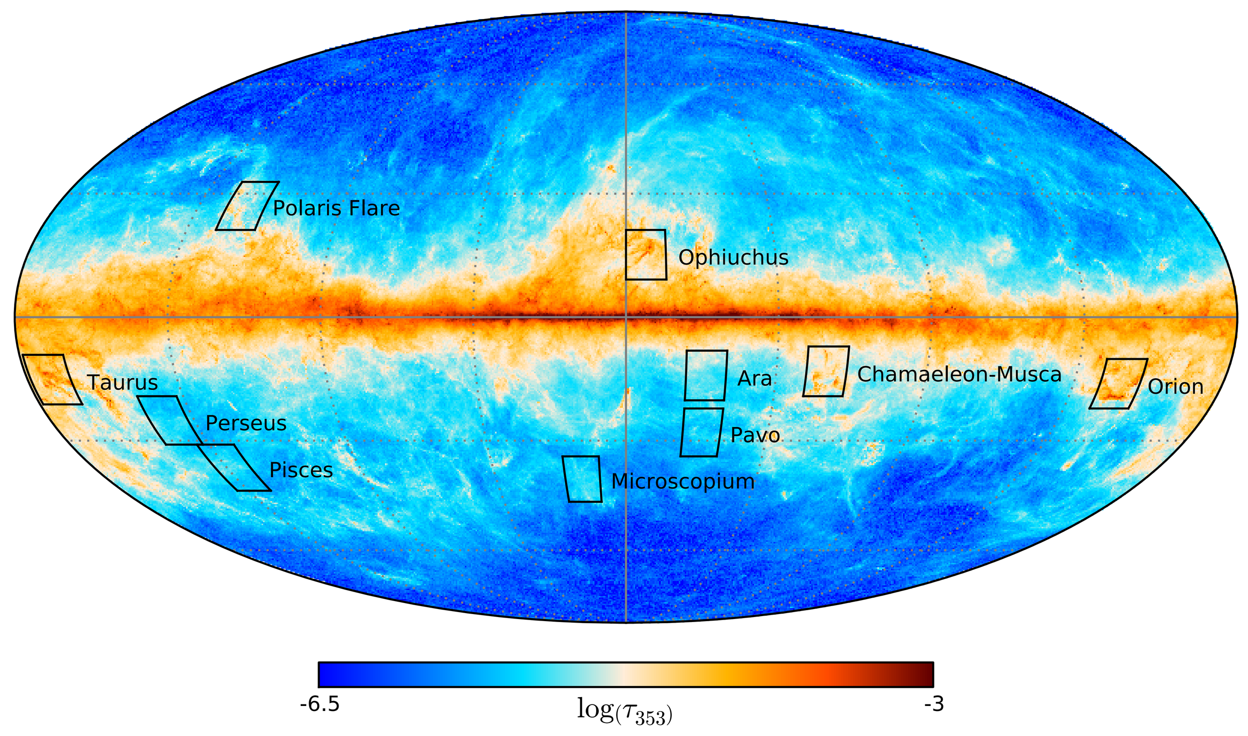

Fig. 1 : Locations of the nearby molecular clouds selected in Planck Intermediate Results XX, overlaid on the map of dust optical depth at 353 GHz, at a 5' FWHM resolution.

1 Polarized dust emission maps

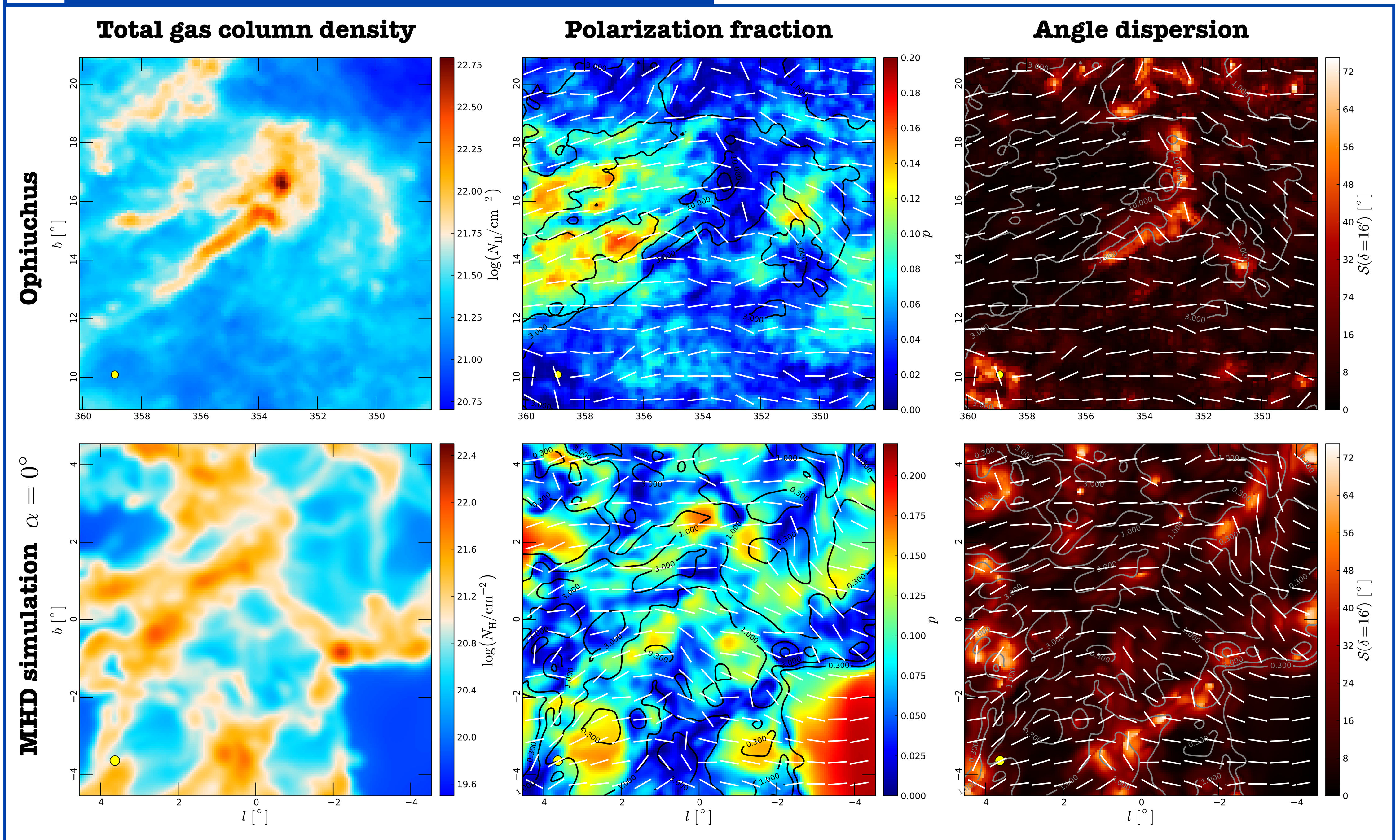

Fig. 2 : Maps of the total gas column density (left), polarization fraction (center), and polarization angle dispersion function (right) in the Ophiuchus field (top row) and in a simulated observation based on a numerical simulation of anisotropic MHD turbulence (bottom row). All maps are at 15' FWHM resolution.

2 Simulating polarized dust emission

We extract a 18 pc x 18 pc x 18 pc subset from a RAMSES (Teysier 2002, Fromang et al. 2006, Hennebelle et al. 2008) simulation of magnetized converging flows of warm (8000 K) atomic gas, which condenses into dense cold structures near the mid-plane. A magnetic field, initially along the gas flows, permeates the medium. We rotate the MHD simulation cube, place it 100 pc away and simulate Stokes I, Q, U maps by integrating along the line of sight. Resulting I, Q, U maps are smoothed at 15' FWHM and simulated polarization fractions and angles are derived, as well as the angle dispersion function.

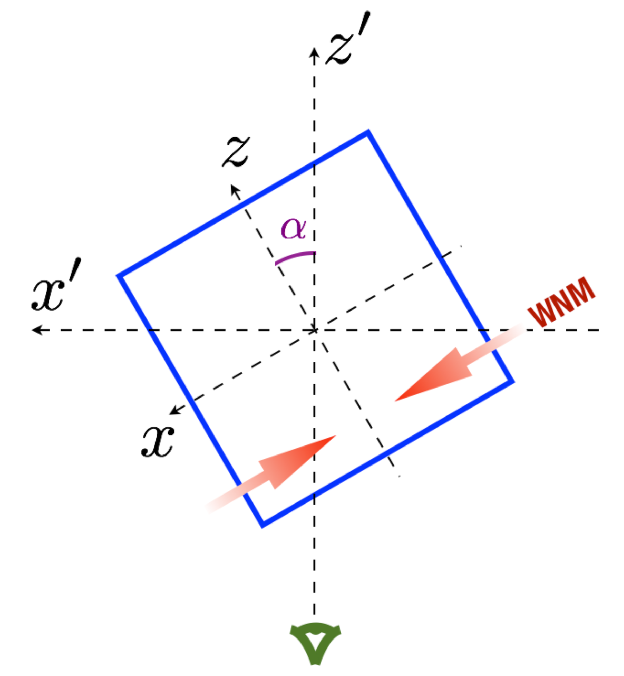

Fig. 3 : The MHD simulation cube is rotated around the y axis, to explore a range of angles between the mean magnetic field and the line of sight. The incoming warm neutral medium flows enter the box parallel to the x axis, and the mean magnetic field in the simulation is along that same axis.

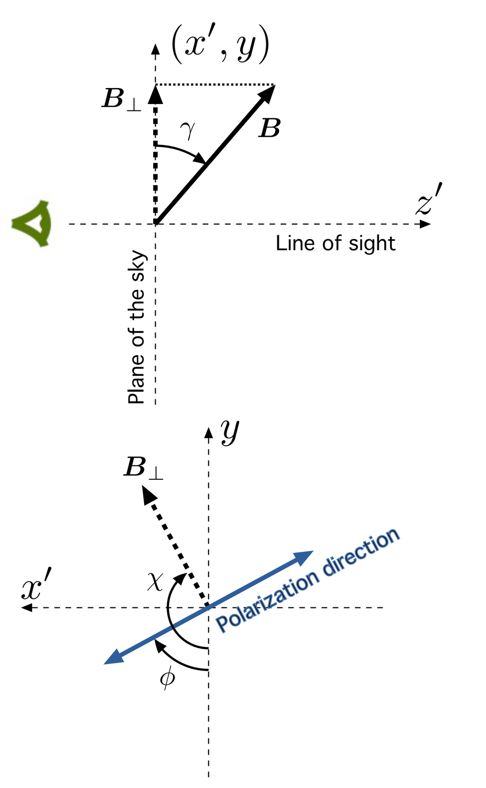

Fig. 4 : Axes and angles notations. Note that the plane-of-the-sky angle used in the definition of the simulated Stokes is that of the polarization vector, not that of the magnetic field.

Stokes parameters

$$I = \int S_\nu e^{-\tau_\nu} \left[1 - p_0 \left(\cos^2\gamma - \frac{2}{3}\right)\right] \mathrm{d}\tau_\nu$$

$$Q = \int p_0 S_\nu e^{-\tau_\nu} \cos(2\phi) \cos^2\gamma \, \mathrm{d}\tau_\nu$$

$$U = \int p_0 S_\nu e^{-\tau_\nu} \sin(2\phi) \cos^2\gamma \, \mathrm{d}\tau_\nu$$

Intrinsic polarization efficiency parameter $p_0 = 0.2$

Dust opacity $\tau_{353}/N_\mathrm{H} = 1.2 \times 10^{-26}\,\mathrm{cm}^{-2}$

Dust temperature $T_\mathrm{d} = 18\,\mathrm{K}$

Derived maps

$$p = \frac{\sqrt{Q^2+U^2}}{I} \qquad \psi = \frac{1}{2}\mathrm{atan}(U, Q)$$

The angle dispersion function is computed over an annulus centered on each pixel

$$\mathcal{S}(\boldsymbol{r}, \delta) = \sqrt{\frac{1}{N}\sum_{i=1}^{N}\left[\psi(\boldsymbol{r}+\boldsymbol{\delta}_i) - \psi(\boldsymbol{r})\right]^2}$$

3 Statistical properties of polarized emission

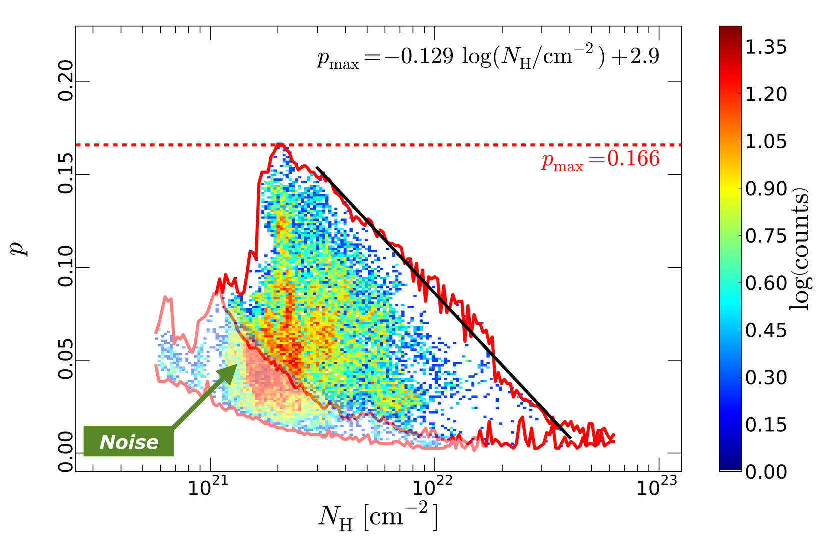

Fig. 5 : Distribution function of polarization fractions and column densities in the Ophiuchus field. The effect of a more stringent threshold in polarization fraction signal-to-noise (3 to 10) is to remove points at the bottom left side.

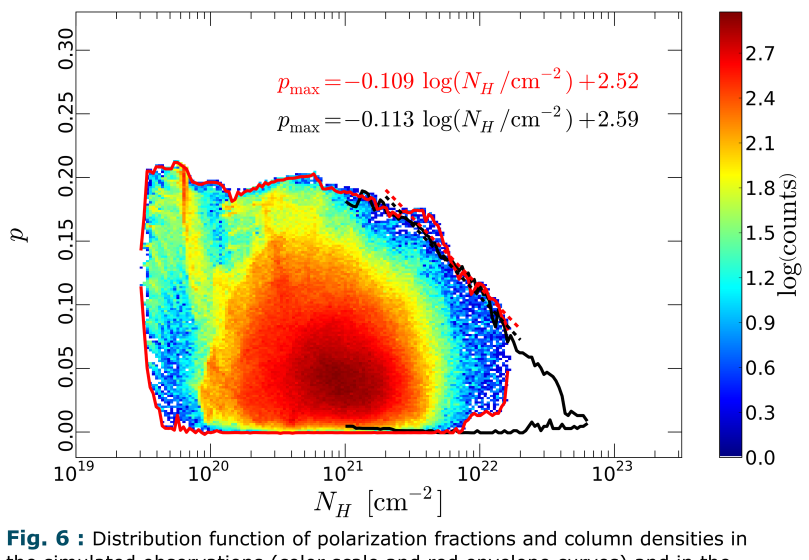

Fig. 6 : Distribution function of polarization fractions and column densities in the simulated observations (color scale and red envelope curves) and in the Planck observations (black envelope curves).

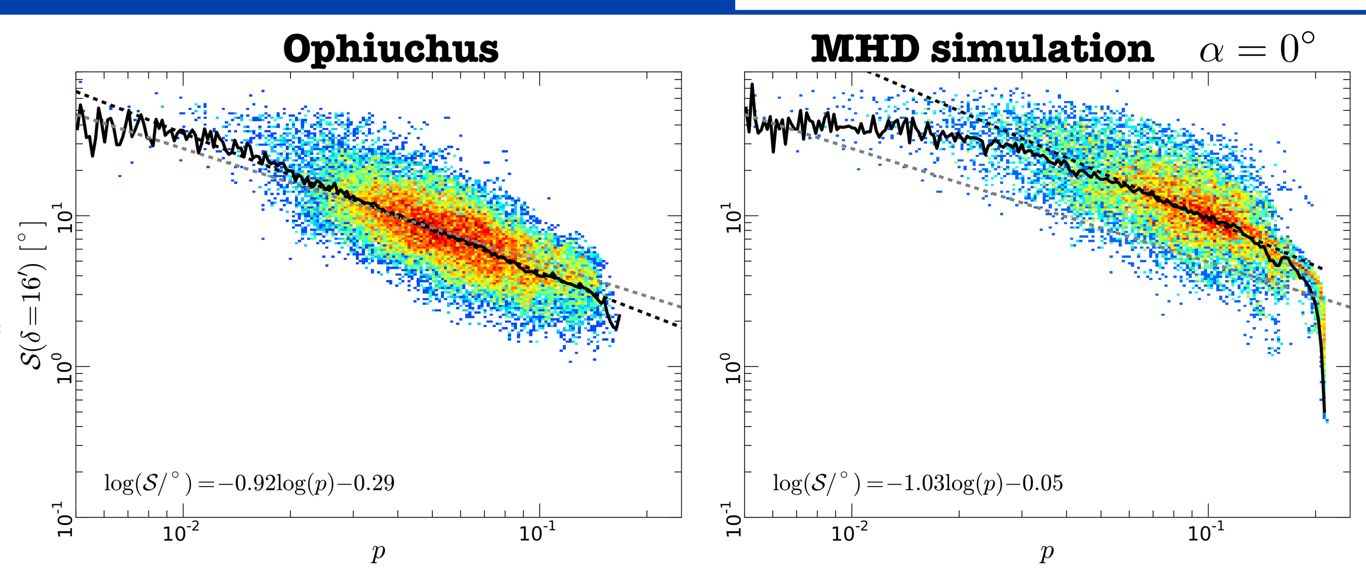

Fig. 7 : Distribution function of polarization fractions and polarization angle dispersion functions in the Ophiuchus field (left) and in a simulated observation (right). The dashed grey line is the large-scale fit, the solid black line shows the mean angle dispersion function per bin of polarization fraction, and the dashed black line is a linear fit of that curve in log-log coordinates, restricted to bins in polarization fraction containing at least 1 percent of the total number of data points.

Field	p_{max}	$p_{max} = m \log(N_H/\mathrm{cm}^{-2}) + c$: m	c	N_H range [10^{21} cm^{-2}]	$\log(\mathcal{S}) = m' \log(p) + c'$: m'	c'
Polaris Flare	0.134 ± 0.015	−0.114 ± 0.014	2.5 ± 0.3	1–4	−0.56 ± 0.08	0.25 ± 0.17
Taurus	0.149 ± 0.011	−0.140 ± 0.004	3.2 ± 0.1	5–25	−0.87 ± 0.09	−0.31 ± 0.11
Orion	0.129 ± 0.014	−0.068 ± 0.003	1.6 ± 0.1	3–40	−0.87 ± 0.11	−0.25 ± 0.13
Chamaeleon-Musca .	0.190 ± 0.008	−0.134 ± 0.003	3.0 ± 0.1	3–20	−0.94 ± 0.03	−0.39 ± 0.02
Ophiuchus	0.166 ± 0.006	−0.129 ± 0.004	2.9 ± 0.1	3–40	−0.92 ± 0.05	−0.30 ± 0.04
Microscopium	0.24 ± 0.05	—	—	—	−0.41 ± 0.07	0.38 ± 0.07
Pisces	0.30 ± 0.11	—	—	—	−0.67 ± 0.13	0.21 ± 0.12
Perseus	0.33 ± 0.09	—	—	—	−0.46 ± 0.09	0.37 ± 0.06
Ara	0.27 ± 0.03	—	—	—	−0.48 ± 0.07	0.15 ± 0.06
Pavo	0.48 ± 0.18	—	—	—	−0.27 ± 0.05	0.57 ± 0.03

Tab. 1 : Polarization statistics in the selected fields : absolute maximum polarization fraction at 15' FWHM resolution and linear fit parameters for the (anti-)correlations between maximum polarization fraction and gas column density on the one hand, and between polarization fraction and angle dispersion function on the other hand.

4 A toy model

In order to gain insight on the statistical properties of the random component of the interstellar magnetic field, we build synthetic observations of polarized dust emission using dust density and magnetic field cubes with controlled statistics.

Dust density : exponentiated fractional Brownian motion field (fBm)

$$n_\mathrm{d} = n_0 \exp\left(\frac{X}{X_r}\right)$$

- Power-law power spectrum with index β_n
- Log-normal distribution
- Possibly large fluctuations

$$\frac{\sigma_n}{\langle n_\mathrm{d}\rangle} = \sqrt{2}\exp\left(\frac{\sigma_X^2}{4X_r^2}\right)\left[\sinh\left(\frac{\sigma_X^2}{2X_r^2}\right)\right]^{1/2}$$

Magnetic field : from fBm vector potential components

$$\widetilde{B_\lambda}(\boldsymbol{k}) = \epsilon_{\lambda\mu\nu} i k_\mu \mathcal{F}_0 |\boldsymbol{k}|^{-\beta_A/2} \exp\left[i\phi_{A_\nu}(\boldsymbol{k})\right]$$

- Power-law power spectrum with index $\beta_B = \beta_A - 2$
- Gaussian distribution with zero mean
- Divergence-free
- Possibility to add a large-scale uniform field

5 Least-squares analysis

Over a range of physical parameters listed in Table 2 (spectral indices of the dust density field and of the magnetic field components, level of density fluctuations, ratio of turbulent to regular magnetic field, and physical depth of the model cloud), we explore the variations of many observables (listed in Table 3) derived from the simulated Stokes maps. We thus build a database relating these physical parameters to selected observables. We can use this database to infer physical parameters from observations based on a least-squares analysis.

Parameter	Prior ranges	Step size	Current step size
β_n	$[2, 5]$	0.2	0.2
β_B	$[2, 5]$	0.2	0.2
$y_n \equiv \sigma_n/\langle n\rangle$	$[0.2, 2]$	0.2	0.4
$y_B \equiv \sigma_{\lVert\vec{B}\rVert}/\langle\lVert\vec{B}\rVert\rangle$	$[0.4, 2]$	0.2	0.4
$d \equiv$ depth	$[1, 120]$	10	20

Tab. 2 : Physical parameters of the input density and magnetic field cubes

Type	From	Method
Spectral index	I, Q, U, P	Fit from power spectrum
Ratio RMS/mean	I, P	Map PDF statistics
Position of PDF maximum	$\Delta\Psi, p, \lVert\nabla\vec{P}\rVert/\lVert\vec{P}\rVert$	Map PDF statistics
Correlation	$\{\Delta\Psi, p\}$ and $\left\{\Delta\Psi, \lVert\nabla\vec{P}\rVert/\lVert\vec{P}\rVert\right\}$	Fit through 2D scatter plot

Tab. 3 : Observables derived from the simulated Stokes maps

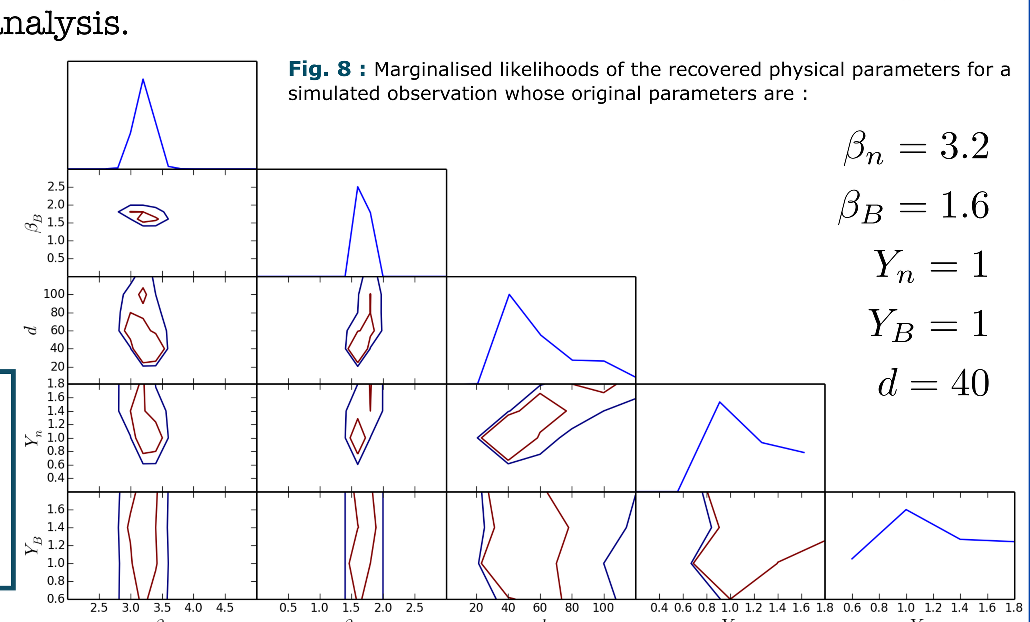

Fig. 8 : Marginalised likelihoods of the recovered physical parameters for a simulated observation whose original parameters are :

$\beta_n = 3.2$

$\beta_B = 1.6$

$Y_n = 1$

$Y_B = 1$

$d = 40$

Conclusions

Towards nearby molecular clouds, the polarization of dust thermal emission at the scales observed by Planck is essentially related to the geometry of the magnetic field. Polarization fractions anti-correlate with column densities, which may be due to a succession of variously polarized structures on the line of sight. They also anti-correlate with the local dispersion of polarization angles. These features are well reproduced by MHD simulations of the diffuse ISM, with comparable correlation coefficients. To go beyond this first analysis, we pursue a least-squares analysis to retrieve the statistical properties of the interstellar magnetic field from Planck observations. Application of this method on a toy model of the turbulent magnetized ISM shows good promise, and we are currently working towards its application on Planck data.

References

Fromang, S., Hennebelle, P., Teyssier, R., 2006, A&A, 457, 371
Hennebelle,P., Banerjee,R., Vazquez-Semadeni,E., Klessen,R.S., Audit,E. 2008, A&A, 486, L43
Planck 2013 Results XI, 2014, A&A, 571, 11
Planck 2015 Results I, A&A submitted
Planck Intermediate Results XIX, 2015, A&A, 576, 104
Planck Intermediate Results XX, 2015, A&A, 576, 105
Teyssier, R., 2002, A&A, 385, 337